An investigation into flashback and blow-off for premixed flames stabilized without a recirculation vortex

Combustion and Flame 235 (2022) 111690

Contents lists available at ScienceDirect

Combustion and Flame

journal homepage: www.elsevier.com/locate/combustflame

An investigation into flashback and blow-off for premixed flames stabilized without a recirculation vortex

F.H. Vance*, Y. Shoshin, L.P.H. de Goey, J.A. van Oijen

Mechanical Engineering, Eindhoven University of Technology, Eindhoven, the Netherlands

ARTICLE INFO

Article history:
Received 2 March 2021
Revised 9 August 2021
Accepted 10 August 2021
Available online 30 August 2021

Keywords:
Flame anchoring
Blow-off
Flashback
Stretch
Heat loss,

ABSTRACT

We have recently shown that premixed CH_4/air flames anchored behind flame holders can stabilize in two flame stabilization regimes characterised by the presence or absence of a recirculation vortex [1]. Focus of the present work is on the underlying mechanisms governing flames anchored without the presence of a vortex for methane-air flames. We revisit the definition of the flame anchoring location and define a new anchoring location which results from flame stretch considerations rather than heat loss considerations. This location can be unambiguously defined for flame holders of different sizes. It is argued that such an anchoring location is more relevant for flames stabilized behind flame holders with sharp corners and do take into account the multi-dimensional nature of heat transfer with the flame holder as well. A quantitative assessment of heat transfer, stretch and preferential diffusion effects is then carried out at the anchoring location for elucidating their impact on the flame speed as a function of the flame holder size. New insights into flame blow-off, flashback and emergence of a recirculation vortex are obtained as a result of this investigation.

1. Introduction

The manner in which a premixed CH_4/air flame stabilizes is crucial for our understanding and the design of burners for different fuels. In practice, one common way to stabilize flames is to use flame holders with sharp corners such as bluff bodies, perforated plates, etc. In our recent work [1], two stabilization regimes have been identified for flames stabilized behind cylindrical flame holders characterized by the presence/absence of a recirculation zone (RZ). We discussed trends of heat loss to the flame holder, flame curvature and flow strain for each of the stabilization regimes. Flames stabilized with a RZ have been discussed widely in the literature [2–13]. In the current study, our objective is to investigate in detail the flame anchoring mechanisms in the absence of a RZ for the cases presented in Ref. [1] in the case of CH_4-air flames and this will contribute to the formation of a generalized overview of the flame anchoring process. This motivation follows the pioneering works by Lewis and von Elbe [14] on the stabilization of premixed flames on flame holders of various sizes. Critical velocity gradient theory of Lewis and von Elbe, however, did not take into account the effects of flow strain, flame curvature, conjugate heat transfer with the flame holder and preferential diffusion effects. As such, researchers are now focusing on numerical simulations for extracting detailed information and understanding the flame anchoring process.

In the stabilization regime characterized by the absence of a RZ, three limit scenarios are of particular interest: 1) flame flashback, 2) flame blow-off, and 3) the emergence of a RZ resulting in the transition to the RZ stabilization regime. In literature, flames stabilized without a RZ received attention in the context of rod stabilized inverted flames, flames stabilized on perforated plates, etc. [14–19]. However, such flames have never been analyzed while taking into account the stabilization regime and for a large variation of flame holder sizes. Such flames can be identified by the following characteristics:

- Merged (continuous) flame fronts at the axis of symmetry near the flame holder,
- High flame curvature at the axis/plane of symmetry,
- Heat loss having the dominating influence on the flame displacement speed at the flame leading edge along the axis of symmetry.

In most of these studies, the geometrical length (radius, distance between slits) of the flame holder is comparable to the flame thickness and consequently merging of the flame fronts at the axis of symmetry results from geometrical considerations. Another consequence of the burner geometry is the presence of higher curva-

* Corresponding author.
E-mail address: f.h.vance@tue.nl (F.H. Vance).

https://doi.org/10.1016/j.combustflame.2021.111690

Nomenclature

r	Radial coordinate
z	Axial coordinate
Y_i	Mass fraction of species i
ω_i	Species source term
$D_{i,m}$	Diffusivity of species i
T	Temperature in Kelvin
λ	Mixture thermal conductivity
c_p	Mixture specific heat
ρ	Mixture density
μ	Mixture viscosity
h	Absolute enthalpy
h_i	Sensible enthalpy of species i
h_i^0	Formation enthalpy of species i
$\mathbf{v}$	Velocity vector
p	Pressure
E	Total energy
ω_T	Heat release rate
$\bar{\bar{\tau}}$	Stress tensor
M_i	Molar mass of species i
$\mathbf{J_i}$	Diffusive flux of species i
Le_i	Lewis number of species i
D	Flame holder diameter
R	Flame holder radius
$\hat{R}$	Flame holder radius scaled with flame thickness
$\hat{r}$	Radial coordinate scaled with flame thickness
$\hat{z}$	Axial coordinate scaled with flame thickness
V_{in}	Inlet flow velocity
$\hat{V}$	Scaled average flow velocity in the region between wall and flame holder
V_{FB}	Flashback limit velocity
V_{BO}	Blow-off limit velocity
V_{TRZ}	Regime transition limit velocity
ϕ	Fuel equivalence ratio
$\hat{z}_{Kmax}$	Axial location of the anchoring location where stretch is the maximum
$\hat{z}_{LE}$	Axial location of the leading edge
K	Flame stretch rate
$\mathbf{u_t}$	Velocity tangent to the flame
$\mathbf{n}$	Flame normal vector
$\S_d$	Flame displacement speed
Ka	Karlovitz integral
κ	Flame curvature
σ	Flame surface area
K_s	Flame stretch due to strain
K_c	Flame stretch due to flame curvature
$\hat{h}$	Scaled total enthalpy
Y	Reaction progress variable
S_L	Unstretched adiabatic flame speed
A_{in}	Inlet area of tube
A_{rim}	Area between the flame holder and the wall
Z_j	Mass fraction of element j
c_j	Sensitivity coefficients
ψ_b	State at the burnt side
s	Flame normal coordinate

ture at the flame base. At this anchoring location, which is also the flame leading edge, the flame speed is affected largely by heat loss effects as it is the closest location to the flame holder. As such any hypothesis that takes into account this point as the anchoring location will conclude that the flame stabilization conditions are met as a result of heat loss, which decreases from the flashback to the blow-off limit. Also, such a location misses the multi-dimensional

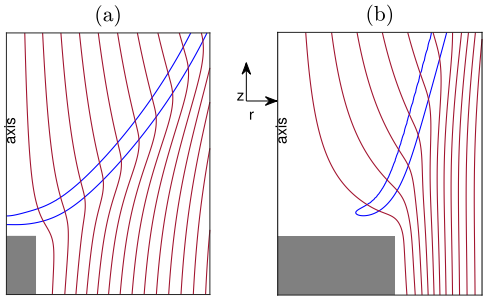

Fig. 1. An illustration of flames stabilized without a RZ with merged (a) and separated (b) flame leading edges at the axis of symmetry near the flame holder. Flame reaction layer location is colored in blue and streamlines in red. (For interpretation of the references to color in this figure legend, the reader is referred to the web version of this article.)

nature of the flame interaction coupled with heat transfer with the flame holder. Counter arguments have already been introduced in Ref. [15] where it is argued that the stabilization of a flame near blow-off with negligible heat loss shows that an adiabatic inverted flame can be stabilized. This paves the way of thinking that flame stretch (strain and flame curvature) is the key influencing factor on flame speed for such flames. An explanation which takes into account one of these effects (i.e. flame curvature) is provided by Kawamuara and co-workers [16,19] and is also favoured by Kedia and Ghoniem [18]. But this reasoning does not take into account the flow strain effects along with the heat circulation through the flame holder. Conditions at flashback are not considered in these studies and as such an analysis from limit (flashback) to limit (blow-off) is missing in the literature.

We have shown in Ref. [1] that near flashback, the contribution from flame curvature dominates the total stretch rate while near blow-off, stretch is caused by both flow strain and flame curvature. Another question that arises is related to the difference between flames with merged and separated leading edges. Two examples are shown in Fig. 1 for a flame holder with a diameter comparable to the flame thickness (Fig. 1a) and a flame holder with a diameter much larger than the flame thickness (Fig. 1b). It can be observed that the flame leading edges are merged for the former case while they are separated in the latter case at the axis of symmetry near the flame holder. When the flame fronts are merged, flame curvature is higher at this location, while it is lower when they are separated. Apart from this difference, the manner in which the flames lose heat to the flame holder could be different. Flames with merged leading edges could lose heat in the flame normal direction while for the separated edges, flames could lose heat in flame normal as well as tangential directions in addition to heat loss from the burnt gases. Apart from these two differences, it can be argued that the two cases are not fundamentally different from each other and as such represent the same stabilization mechanism with differences resulting from flame holder geometry. These arguments serve as the basis for Section 3 of this paper, where justifications for a different flame anchoring location are presented, which gives a clearer idea about the flame stabilization process.

In order to analyze such flames, we first identify the region at the flame base that governs the flame anchoring process when a RZ is not present. Then we use the flame stretch theory of de Goey and ten Thije Boonkkamp [20] for a quantitative assessment of different contributions from direct stretch, enthalpy changes and preferential diffusion terms to the density weighted flame displacement speed $S_{D,b}$ (at the burnt side of flame) for flame holders of varying radii. This separation is our guide for further understanding the flame stabilization mechanism. The main objectives of this study are to:

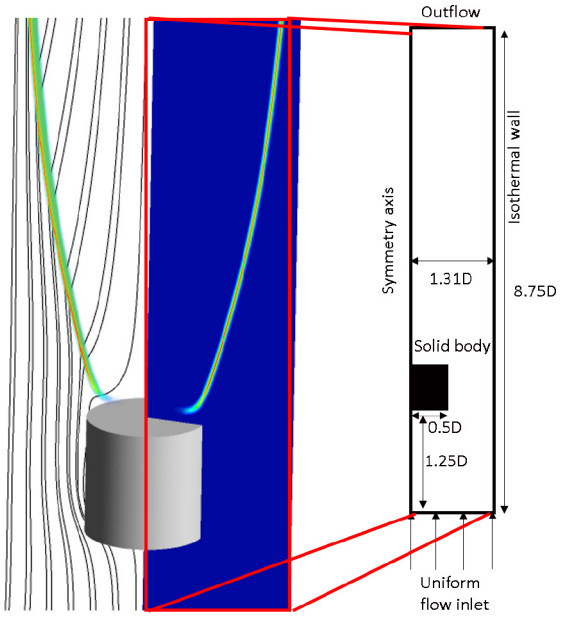

Fig. 2. Left side: Flame stabilized on a cylindrical flame holder. Flame is represented by heat release rate contour (colored), streamlines by black lines and bluff body by the grey cylinder. Right side: Computational model used in this study with D=8 mm.

- Identify a physical and consistent location in the flame that governs the mechanism of flame anchoring for flame holders of various sizes. We will call this location as the anchoring location.
- Understand the role of different contributions to the flame displacement speed $S_{D,b}$ at the anchoring location when approaching flame flashback, blow-off and transition to the RZ stabilized regime limits for flame holders of different sizes.

The structure of this paper is as follows: In Section 2 the numerical model is introduced. In Section 3 the location of the flame anchoring point is discussed. Section 4 introduces the flame stretch theory used to analyze flames at the anchoring location and an analysis of the contributions to the flame speed at the anchoring location for flame flashback, blow-off and regime transition limits is presented.

2. Numerical model

The numerical model used in this study is the same as employed in our previous study [1] on stabilization regimes and a schematic of this setup is shown in Fig. 2. A brief description is given here and other details can be found in Ref. [1,12,21]. The geometry consists of a cylindrical bluff body with radii $R = D/2$ varying from 0.5 mm to 4 mm, placed concentrically inside a cylindrical glass tube with radius of 10.5 mm. An axi-symmetric 2D slice of this geometry is modelled for the solid (flame holder) and fluid domains. The wall of the enclosing tube is modelled as an isothermal no-slip wall with a temperature of 300 K. The outlet is modelled with a Neumann type boundary condition implying that there is no change in the field variables in the normal direction. Conjugate heat transfer of the fluid with the solid bluff body (thermal conductivity, $k = 109$ W/K m) is also modelled. The steady equations are solved using the SIMPLE solver with a finite volume solver and a second-order upwind discretisation scheme using the commercial software package Ansys Fluent [22]. The mixture consists of a CH_4/air and the fuel equivalence ratio ϕ is fixed at 0.68 throughout this study. The chemistry for CH_4/air flames is modelled using the DRM19 mechanism [23] which contains 21 species and 84 reactions. Constant Lewis number based mixture properties are used [24,25]. Constant Lewis numbers are calculated by simulating one-dimensional flat flames using mixture-averaged properties using CHEM1D [26] are shown in Tab. 1. For a steady, laminar, reactive flow, the following equations are solved for an axisymmetric domain:

Table 1
Lewis numbers used in the numerical simulation for CH_4-air flames at $\phi = 0.68$.

Species	*Le*
H_2	0.317
H	0.189
O	0.712
O_{rm2}	1.087
OH	0.736
H_2O	0.854
HO_2	1.078
CH_2	1.023
CH_2^*	1.022
CH_3	1.049
CH_4	1.043
CO	1.171
CO_2	1.404
HCO	1.314
CH_2O	1.329
CH_3O	1.360
C_2H_4	1.402
C_2H_5	1.550
C_2H_6	1.546

$$\nabla \cdot (\rho \mathbf{v}) = 0, \tag{1}$$

$$\nabla \cdot (\rho \mathbf{v} Y_i) + \nabla \cdot \mathbf{J}_i = \omega_i, \tag{2}$$

$$\nabla \cdot (\rho \mathbf{v}\mathbf{v}) = -\nabla p + \nabla \cdot \bar{\bar{\tau}}, \tag{3}$$

$$\nabla \cdot ((\rho E + p)\mathbf{v}) = \nabla \cdot (\lambda \nabla T) - \nabla \cdot (\Sigma_i h_i \mathbf{J}_i) + \omega_T. \tag{4}$$

In the above equations, the velocity vector, density, the species mass fractions, the species source terms, pressure, temperature and species sensible enthalpy are represented by $\mathbf{v}$, ρ, Y_i, ω_i, p, T, and h_i respectively. The stress tensor, total energy, enthalpy and thermal heat release rate are represented by $\bar{\bar{\tau}}$, E, h and ω_T, respectively and are given by

$$\bar{\bar{\tau}} = \mu[(\nabla \mathbf{v} + \nabla \mathbf{v}^{\mathbf{T}}) - \frac{2}{3}\nabla \cdot \mathbf{v} I], \tag{5}$$

$$E = h - \frac{p}{\rho} + \frac{\mathbf{v} \cdot \mathbf{v}}{2}, \tag{6}$$

$$h = \sum_i Y_i h_i, \tag{7}$$

$$h_i = \int_{T_{ref}}^{T} c_{p,i} dT, \tag{8}$$

$$\omega_T = \sum_i \frac{h_i^0}{M_i} \omega_i. \tag{9}$$

Here, formation enthalpy and molecular weight of species i is represented by h_i^0 and M_i, respectively. $\mathbf{J}_i$ represents the Fickian diffusion flux and is given by

$$\mathbf{J}_i = -\rho D_{i,m} \nabla Y_i. \tag{10}$$

Here $D_{i,m}$ are the mixture averaged Fickian diffusion coefficients for species i. Diffusion due to thermal gradients has been ignored

in this study. The transport properties are calculated based on the following relations [25]:

$$\lambda = 2.58e-5c_p\left(\frac{T}{298}\right)^{0.69}[\mathrm{Wm^{-1}K^{-1}}] \quad (11)$$

$$\mu = 1.67e-8c_p\left(\frac{T}{298}\right)^{0.51}[\mathrm{kgm^{-1}s^{-1}}] \quad (12)$$

Here the mixture viscosity, conductivity and the specific heat capacity is represented by μ, λ and c_p, respectively. The reacting flow equations are solved on an equidistant structured grid with a 100 μm global grid resolution. A two-level grid refinement is applied based on the temperature gradient resulting in a local resolution of 25 μm in the flame zone. These mesh resolutions proved to give well resolved and grid independent solutions [1,12]. Flames are established by igniting a high temperature patch near the rear end of the flame holder for one case for each flame holder and then using this result as an initial condition for increasing (for finding the blow-off limit) and decreasing (flashback limit) inlet flow velocities. We have previously validated our model with experiments in Ref. [12] by comparing flame shape and burning profiles. A further validation of the numerical model is provided here by comparing velocity profiles from numerics with that measured using Particle Image Velocimetry method (PIV) at different locations above the bluff body flame holder. The mixture was seeded with Al_2O_3 particles with an average size of approximately $1\mu m$ using a custom-made fluidized bed seeding system. The flame region was illuminated by a 0.5 mm thick light sheet of an Nd:YAG dual pulsed laser (Brio, Quantel) with a wavelength of 532 nm, and images were taken by a 1 megapixel PIV camera. In order to eliminate the background reflection of the laser light, the back part of the inner wall of the protective quartz tube was painted with thermal resistant black paint. Mass flow controllers used in the experiment have an accuracy of 1%. A comparison between axial and radial velocity profiles at different axial locations from the top of the flame holder is presented in Fig. 3 for a mixture velocity of $1\,\mathrm{ms^{-1}}$ and flame holder with $R = 4$ mm. We can observe an excellent agreement between the axial velocity profiles from numerics and PIV measurements. The flow profiles confirm the symmetric nature of the flow in the presence of the flame although the non-reacting flow would be unsteady as the Reynolds number is about 500. Another observation can be made for the absence of any significant negative axial velocity near the flame holder, showing that an recirculation zone is absent. For radial velocity profiles, a mismatch between simulation and experimental results can be observed at $z/D = 0.05$ possibly caused due to the difficulty in experiments in measuring flow near walls. For the locations further downstream, a good agreement can be observed again. It can be concluded from this section that results from numerical simulation and PIV measurements are in excellent agreement with each other and the model can be used with confidence for further investigating flame stabilization mechanisms.

The blow-off limit is characterized by the flame convecting out of the domain and the flashback limit is characterized by stabilization of the flame at an undesired location upstream of the flame holder. The transition to recirculation zone (RZ) stabilized flames is characterized by an immersion of the flame base inside the vortex above the cylinder once it emerges at higher velocities. The eight cylindrical flame holders of different sizes studied in this paper are presented in Table 2. Blow-off V_{BO}, flashback V_{FB} velocity limits and the limit V_{TRZ} at which flame transitions to the RZ stabilized regime are also shown in Table 2. They are defined as the last V_{in} for which a stable flame without a RZ is observed using the numerical model. The velocities at which flashback and blow-off were observed, respectively, are shown in brackets. A non-dimensional radius of the flame holder is also defined in Tab. 2 as $\hat{R} = \frac{D}{2\delta_F}$ with

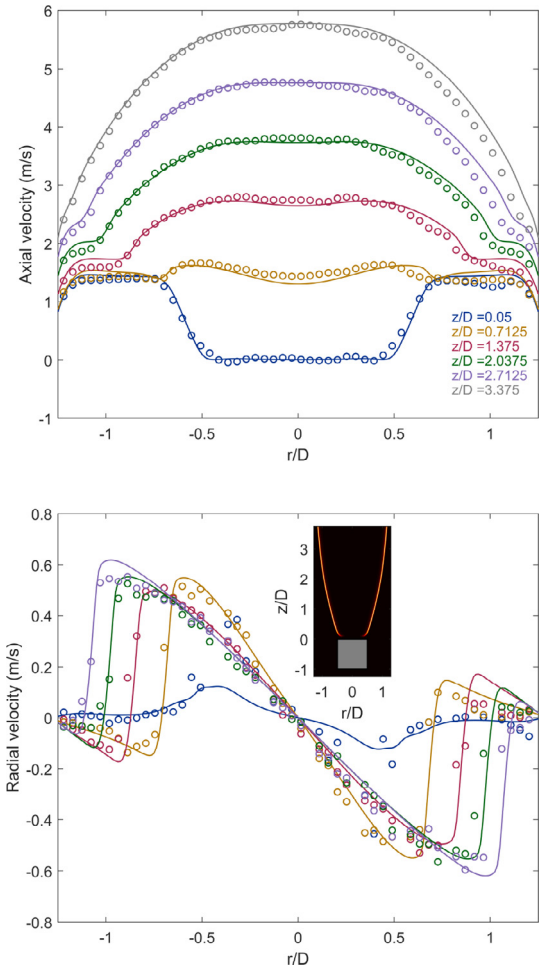

Fig. 3. A comparison between axial (top) and radial (bottom) velocity component from numerical simulations and experimental PIV measurements for $\phi = 0.68$ and $V_{in} = 1\,\mathrm{ms^{-1}}$ and $D = 2R = 8$ mm. Solid lines show the results from numerical simulations and ○ mark PIV measurements. Heat release rate contours for the corresponding flame is added in the bottom figure.

$\delta_F = 0.635$ mm, being the flame thickness computed using the definition based on maximum temperature gradient [27] for a corresponding 1D flat flame at $\phi = 0.68$. It can be observed that flashback limits are almost the same for all flame holders while the blow-off limit increases as the radius of the flame holder is increased. Regime transition velocity V_{TRZ} also remains constant even though Reynolds numbers are different for each flame holder. This indicates that the regime transition is a function of V_{in}/S_L rather than the Reynolds number. The global analysis of limits of stabilization when a RZ is not present from Table 2 indicates major trends but what is of interest here is the underlying mechanisms that cause these limits to exist in terms of contributions from stretch, preferential diffusion and heat transfer with changing flame holder radii. For this purpose, in the next section, a comprehensive discussion on a consistent and physical anchoring location is presented.

3. Flame anchoring location

In this section, an anchoring location is identified that takes into account the multi-dimensional nature of the flames presented here. In the literature of inverted rod stabilized flames, the positively curved flame leading location is usually taken as the anchoring point [15,16,18,19,28] for explaining unstable flame behaviour. However, in such analyses, no discussions are provided for the

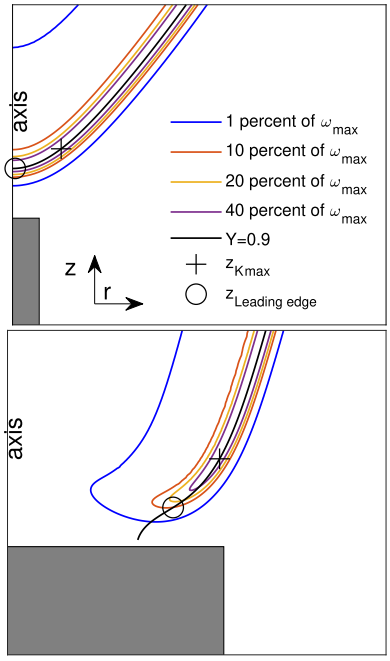

Fig. 4. Various isolevels of heat release rate along with isolevels of reaction progress variable Y in the inner layer of the flame structure. Location where stretch is maximum is marked with + symbol while the leading edge is marked with ○ symbol. $\omega_{\max}$ is the maximum heat release rate. Top plot: $\hat{R} = 0.79$, $\hat{V} = 3.40$. Bottom plot: $\hat{R} = 6.30$, $\hat{V} = 6.10$.

choice of this point and it is usually assumed to be the flame anchoring location, possibly due to the simpler 1D nature of the flow profile at the axis of symmetry. Another problem is related to the situation when there is no clear flame leading edge as the flame base has separated fronts for larger radii of the flame holder.

In order to define a flame leading edge, various isolevels of heat release rate are plotted in Fig. 4 for merged and separated flame leading edges. Iso-levels of progress variable (defined as $Y = \frac{Y_f - Y_{f,u}}{Y_{f,b} - Y_{f,u}}$, where Y_f is the methane mass fraction) in the inner layer of the flame structure with $Y = 0.9$ are also plotted. It can be observed that when the flame fronts are fully merged at the base of the flame, the leading edge is easy to define as the most upstream point on the isocontour $Y = 0.9$ near the flame holder, marked by ○. Here, the flame leading edge location can be specified by a z axial coordinate location. For separated flame fronts, this flame inner layer isolevel is not aligned with the reaction rate fronts due to flame tangential fluxes in the quenching region. The flame leading edges in this case are defined as the most upstream location in the flame inner layer where it intersects the isocontour of 10% of the maximum heat release rate. This point is marked by ○ in the right panel of Fig. 4. It is noted here that other values of heat release rate could also be used resulting in a arbitrariness in selection of the flame anchoring location due to vanishing of heat loss and stretch effects at downstream locations. The leading edge location for separated flame fronts is characterized by r and z coordinates and forms a circle due to the cylindrical geometry. However, the flame leading edge where the heat loss dominates other effects and flame curvature reaches its maximum level, is not the only location that can act as the flame anchoring location. Another location which can govern the flame anchoring process is the location at the inner layer of the flame where the stretch rate is maximum $K_{\max}$ along the axial length. This location is marked by + symbols in Fig. 4 and is the focus of this section. This is a clear and unique location and therefore, more relevant to flame anchoring.

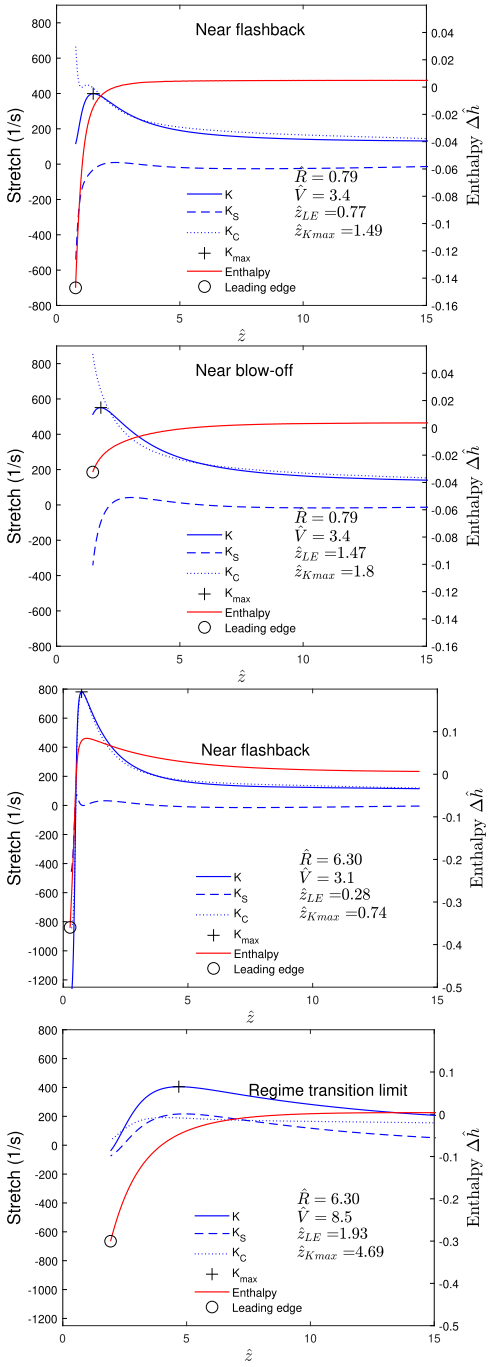

Fig. 5. Total stretch K, contributions from flow strain K_S and flame curvature K_C and enthalpy at the inner layer of the flame. The location of maximum stretch is marked with + symbol while leading edge location is marked by ○ for flashback and blow-off limit flames for $\hat{R} = 0.79$ and $\hat{R} = 6.3$.

In order to analyze further, a plot of normalized enthalpy and stretch rate (along with strain and curvature contributions) at the inner layer of the flame are shown in Fig. 5 for flashback and blow-off limit flames for the smallest $\hat{R} = 0.79$ and largest $\hat{R} = 6.3$ flame holders presented in Ref [1]. Here $\hat{V} = \frac{A_{inlet}}{A_{rim}} \frac{V_{in}}{S_L}$ is the average flow velocity in the region between the flame holder and the wall, normalized with the adiabatic unstretched flame speed. Here A_{inlet} and A_{rim} are the area of the tube inlet and area between flame holder and tube outer wall. The enthalpy, h is made dimensionless as

$$\hat{h} = \frac{h - h_{in}}{c_{p_u}(T_b^0 - T_u)}, \tag{13}$$

where h is the local total enthalpy, T_u is the unburnt mixture temperature, c_{p_u} the specific heat capacity of the unburnt mixture and T_b^0 is the burnt temperature for the corresponding adiabatic unstretched flame. The difference $\hat{\Delta h}$ between $\hat{h}$ at the inner layer of the flame, i.e. the non-ideal 2D flames presented here and $\hat{h}$ for 1D ideal flat flame, is shown in Fig. 5. The stretch rate, K, calculated for stationary flames using $K = \nabla_t \,.\, \mathbf{u_t}$, where ∇_t is the flame tangential component of the ∇ operator, $\mathbf{v}$ and $\mathbf{n}$ are local flow velocity and flame normal vector with $\mathbf{u_t}$ being the tangential component of the gas velocity [27]. The flame stretch rate K contains contributions from flow strain K_S along with flame curvature effects K_C. Curvature K_C and strain contribution K_S are calculated following Ref. [27,29]:

$$K_C = -S_d(\nabla_t \cdot \mathbf{n}), \tag{14a}$$

$$K_S = \nabla_t \cdot \mathbf{v}, \tag{14b}$$

where S_d is the local displacement speed given as $S_d = -\mathbf{v} \cdot \mathbf{n}$. Total stretch K, stretch due to flow strain K_S and curvature induced stretch K_C is plotted in Fig. 5. It can be observed that for relatively small flame holders like $\hat{R} = 0.79$ at the flame leading edge, heat loss and curvature-induced stretch rate are maximum for each case. The enthalpy is more negative for the flashback limit case than for the blow-off limit case. There is also a negative flow strain rate, which decreases the total stretch rate. Just downstream of this leading edge, the flame stretch rate reaches a maximum value along the flame front because the flow strain becomes slightly positive. This location of maximum stretch rate $K_{\max}$ is present in all the flames observed in this and our previous study [1] and can be of universal nature for flames stabilized behind cylindrical flame holders without a recirculation zone. For the larger $\hat{R} = 6.3$ flame holder, at the flashback limit, similar trends for strain and enthalpy can be observed as well. However, at the leading edge, the curvature contribution is negative and reaches a maximum value at the location of $K_{\max}$ coupled with the maximum value of $\Delta\hat{h}$, indicating strong pre-heating effects at this location. For $\hat{V} = 8.5$, at the transition to the RZ regime limit for $\hat{R} = 6.3$, strain and flame curvature contribute to the total stretch in similar magnitudes and the $K_{\max}$ location shifts further downstream.

From the discussion above, it seems that the location where the stretch rate is maximum in the inner layer of the flame along the flame length is inherent to flames stabilized behind bluff body type flame holders along with the quenching point/leading edge. As such, it gives sufficient reason for continuing our investigation about this location as the flame anchoring location in the next subsections.

3.1. Stabilization of an adiabatic but stretched flame

In order to further investigate the importance of stretch compared to heat loss in the stabilization of premixed flames behind flame holders presented here, a numerical simulation is performed with no heat loss to the flame holder for $\hat{V} = 3.4$, $\hat{R} = 0.79$, which is the blow-off limit case for the respective flame holder. This is done by applying a zero heat flux boundary condition on the flame holder geometry in the numerical simulation. The simulation without heat loss is carried out to give an indication about the importance of stretch on flame stabilization. If heat loss is of prime importance, the flame should not stabilize and blow-off instead in this scenario. Otherwise, if stretch is of primary interest, then the flame will find a new anchoring location in order to compensate for contribution from heat loss, resulting in a stable flame.

Results of heat release rate with locations of the flame leading edge and $K_{\max}$ are shown in Fig. 6 for the two cases. Stabilization of the flame without heat loss shows that it is possible to stabilize

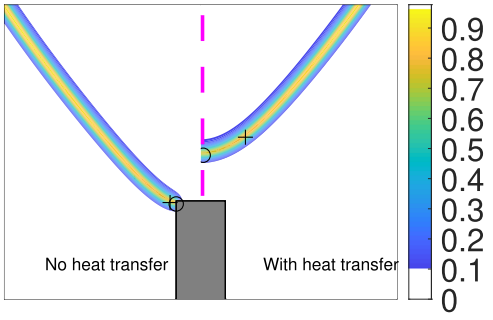

Fig. 6. Heat release rate contours for the blow-off limit flame for $\hat{R} = 0.79$ and $\hat{V} = 3.4$ without and with heat transfer to the flame holder. The location of maximum stretch is marked with + symbol while leading edge location is marked by ◦.

an adiabatic flame, which puts emphasis on the argument that the stretch rate is the primary contributor towards lowering flame displacement speed at the anchoring location near the flame holder. It can be observed that without heat loss, the flame leading edge stabilizes on the corner of the flame holder and the $K_{\max}$ location lies immediately downstream of this location. The close proximity of these two points shows that without heat loss the flame anchoring location can be solely described by the $K_{\max}$ location.

Local plots of the flame stretch rate are shown in Fig. 7 for the flame without heat loss. This plot can be compared with the second from top plot in Fig. 5 where heat transfer with the flame holder was enabled. It can be observed that the stretch rate is maximum in close proximity to the flame leading edge. Stretch consists almost entirely out of flame curvature while a small flow strain part is also present. The enthalpy decreases because of slight Lewis number effects present in lean CH_4-air flames.

This subsection shows that in the case of no heat loss, the flame can adjust its flame speed by moving closer to the flame holder and stabilize solely due to flame stretch. This result can be interpreted to show that flame stretch acts as a primary factor for non-flat flames stabilized on bluff bodies and thus an anchoring location defined based on such considerations can result in a more physical outlook of the stabilization process.

3.2. Visualization of the anchoring location and heat transfer with the flame holder

In this subsection, the changes in the flame leading edge location along with the location of maximum stretch with respect to heat circulation through the flame holder are visualized. Main objective is to show that the location of maximum stretch can also take into account effects of heat loss as well as pre-heating from the side walls. The heat release rate along with markers for different anchoring points as well as a pre-heating iso-level and a heat loss iso-level are plotted in Fig. 8. The top row shows results for the smallest flame holder with $\hat{R} = 0.79$. It can be observed that with increasing $\hat{V}$, the flame moves away from the flame holder resulting in less heat loss to the flame holder marked by the red line. The pre-heating iso-level marked by the blue lines, shows the resulting heat transferred back to the flame via the flame holder. The area occupied by the blue line decreases from the flashback to the blow-off limit in accordance with the decrease in net heat loss with increasing $\hat{V}$. Consequently, the flame front at the $K_{\max}$ location is less supported by the pre-heating at higher velocities.

Results for the $\hat{R} = 1.57$ flame holder are shown in the second row of Fig. 8. A similar trend can be observed for the flame stand-off distance and anchoring locations along with stretch rate and enthalpy contribution as for $\hat{R} = 0.79$. In this case, the flame moves further away from the flame holder when increasing the mixture velocity. The blow-off limit for $\hat{R} = 1.57$ is higher than that for $\hat{R} =$

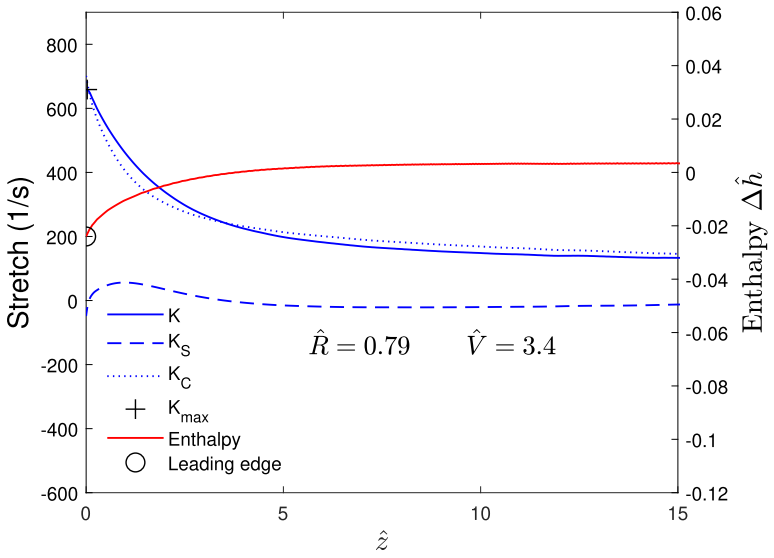

Fig. 7. Total stretch K, contributions from flow strain K_S and flame curvature K_C and enthalpy at the inner layer of the flame for $\hat{V} = 3.4$, $\hat{R} = 0.79$ without heat loss to the flame holder. The location of maximum stretch is marked with a + symbol while the leading edge location is marked by ∘.

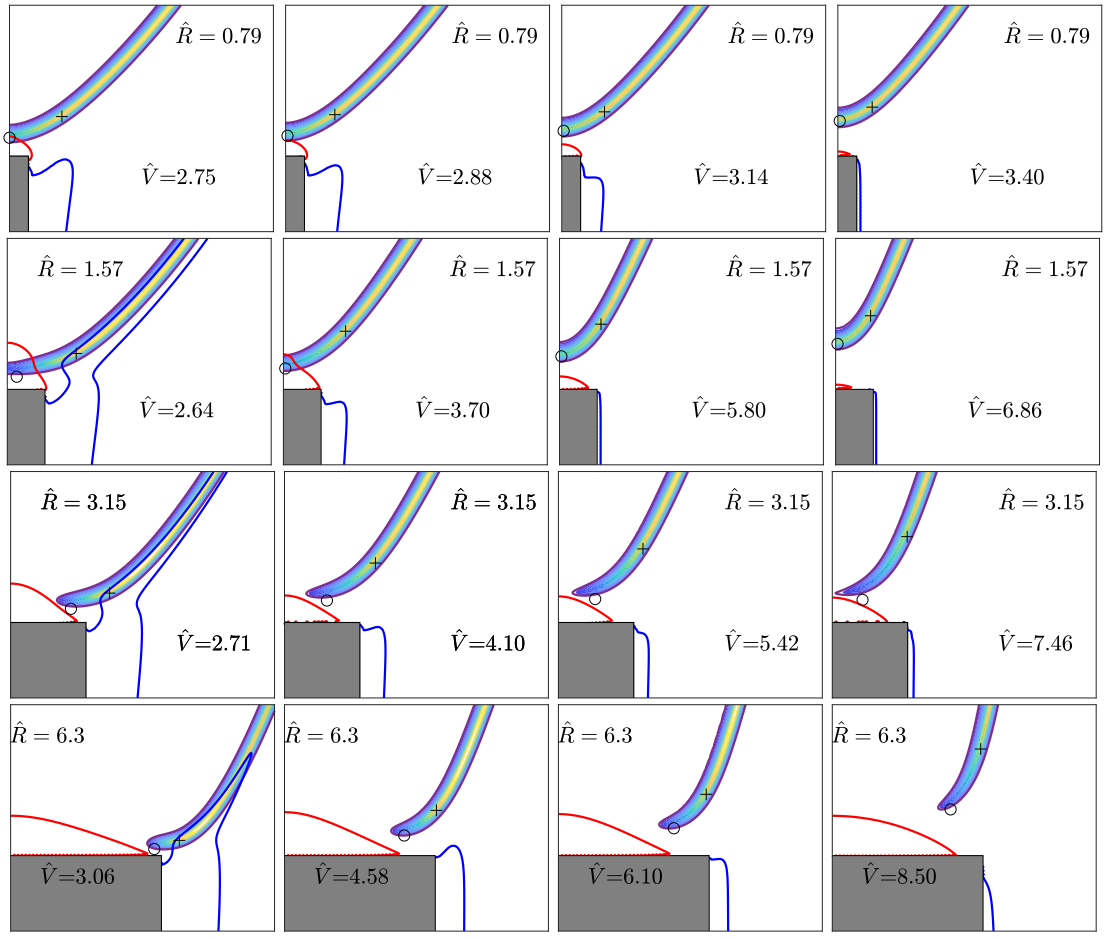

Fig. 8. Flame anchoring locations for increasing $\hat{V}$ from flashback to blow-off. Heat release rate contours are shown along with the leading edge location (∘ symbol) and K_{max} location (+ symbol) for $\hat{R} = 0.79, 1.57, 3.15$ and 6.3 flame holders. Pre-heating (blue) ($\hat{h} = 0.01, 0.02, 0.04, 0.08$ for $\hat{R} = 0.79, 1.57, 3.15, 6.3$) and heat loss (red) iso-levels are also shown ($\hat{h} = -0.1, -0.2, -0.4, -0.6$ for $\hat{R} = 0.79, 1.57, 3.15, 6.3$). (For interpretation of the references to color in this figure legend, the reader is referred to the web version of this article.)

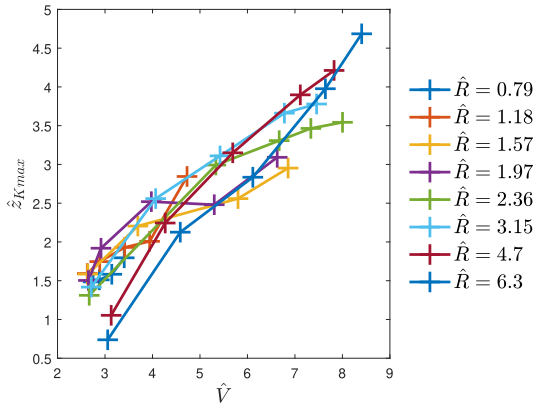

Fig. 9. Variation of anchoring location where the stretch is maximum $\hat{z}_{Kmax}$ for all the flames presented in Table 2 as a function of scaled velocity $\hat{V}$.

0.79. This difference results from an increase in the surface area of the burner resulting in higher heat transfer which provides pre-heating support to the $K_{\max}$ flame region for a wider range of $\hat{V}$ values than for $\hat{R} = 0.79$.

Similar observations can also be made for $\hat{R} = 3.15$ and 6.3 flame holders in Fig. 8 where $\hat{h} = 0.04$ and 0.08 isolevels are shown for marking pre-heating while $\hat{h} = -0.4$ and -0.6 isolevels are shown for marking heat loss, respectively. In these cases, the flame leading edges are clearly separated due to a flame holder radius which is larger than the flame thickness. Despite this, a similar behaviour of the flame leading edge (moving away from the flame holder) and $K_{\max}$ region (also moving away from the holder) can be observed when compared with the joint flame fronts for smaller flame holders. The heat loss contours (red lines) appear to change less with $\hat{V}$ than they did for smaller flame holders. This difference is caused by the presence of burnt gases in between the separated flame leading edges, that lose heat to the flame holder. This heat loss from the burnt gas is directly proportional to the surface area of the flame holder top surface [1]. For the flame holder with the lowest radius in our study, bluff body temperature decreases from 369 K at flashback limit to 313 K at the blow-off point while for the largest flame holder, temperature decreases from 734 K at the flashback limit to 457 K at the regime transition limit.

3.3. The flame anchoring location

It has been argued in the previous subsections that the presence of a maximum stretch location is of key importance to the flames stabilized behind flame holders with sharp angles at corners due to geometrical considerations and flow behaviour. The maximum value of the stretch rate $K_{\max}$ results from a combination of flame curvature and flow strain effects and exists just downstream of the flame leading edge. It is also argued that the location where the stretch rate is maximum is physically more relevant as the anchoring point than the leading edge and describes flame stabilization for flame holders of all investigated sizes thus resulting in a more consistent definition as well. It also takes into account the heat transfer with the flame leading edge via circulation through the flame holder. Therefore, this location is adopted as the anchoring point for the investigation of the limits of flames stabilized without a RZ. The spatial position of this anchoring point $\hat{z}_{Kmax}$ is shown in Fig. 9 as a function of scaled velocity $\hat{V}$ for all the cases simulated in this study. The lowest $\hat{V}$ represents the flashback limit while the highest value of $\hat{V}$ represents either the blow-off or regime transition limit. It can be observed that $\hat{z}_{Kmax}$ is a strong function of flow velocity as also observed in Fig. 8. The

Table 2
Flashback, blow-off velocity and regime transition limits for flame holders of different diameter (D) at $\phi = 0.68$. $\hat{R} = \frac{D}{2\delta_F}$. Values outside of brackets represent the limits while values inside the brackets indicate velocities at which flashback, blow-off and regime transition occurred, thus indicating the accuracy of the limit calculation process.

D [mm]	$\hat{R}$	V_{FB} [ms^{-1}]	V_{BO} [ms^{-1}]	V_{TRZ} [ms^{-1}]
1	0.79	0.51 (0.50)	0.675 (0.70)	–
1.5	1.18	0.50 (0.45)	0.9 (1.00)	–
2	1.57	0.50 (0.45)	1.3 (1.40)	–
2.5	1.97	0.50 (0.45)	–	1.375 (1.50)
3	2.36	0.50 (0.45)	–	1.375 (1.50)
4	3.15	0.50 (0.45)	–	1.375 (1.50)
6	4.7	0.55 (0.50)	–	1.375 (1.50)
8	6.3	0.50 (0.45)	–	1.375 (1.50)

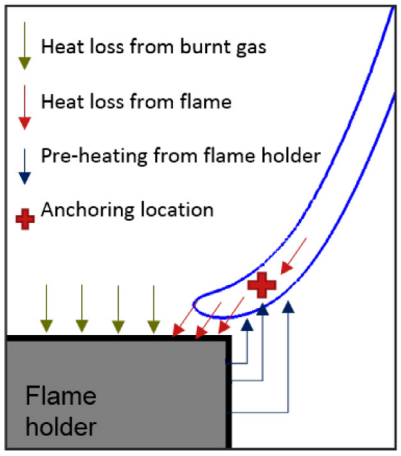

Fig. 10. An illustration of heat transfer around the anchoring location where stretch rate is maximum.

flame anchoring location moves closer to the flame holder almost monotonically for all flame holder sizes, as the flow velocity is decreased and vice versa when the velocity is increased. It is to be noted that the value of $\hat{z}_{Kmax}$ is a consequence of the flame-flow kinematic balance for a set of conditions. If these conditions are changed, the flame is expected to move in the vicinity of the flame holder to find a new balance (if it cannot find a new balance it will flashback, blow-off or transit to the RZ regime). Our hypothesis in this study is that the movement of the maximum stretch location can represent the dynamics of the flame anchoring process resulting from underlying changes in the flame speed.

It is to be noted here that it is not argued in this study that heat loss is not important in flame stabilization, rather it is argued that stretch is the primary contributor towards flame stabilization and heat loss acts as secondary contributor. The flame anchoring location model is illustrated in Fig. 10 for a case with separated flame fronts, focusing on the heat transfer around the anchoring location where flame stretch is maximum. The effect of heat transfer is more manifest at the location of maximum stretch, which takes into account the associated pre-heating support (or lack of it) from the flame holder side walls. It is also to note that the maximum stretch location could still be largely affected by a net heat loss. In the next sections, we will use the flame stretch theory to separate individual contributions from stretch, preferential diffusion and enthalpy changes at the anchoring location for eight different flame holders presented in Tab. 2.

4. Separating contributions to the flame speed using flame stretch theory

For steady flames, flame displacement speed can be calculated from the kinematic balance $m = -\rho(\mathbf{v}\cdot\mathbf{n}) = \rho S_d$, where ρ is the density, $\mathbf{v}$ is the local gas velocity, $\mathbf{n}$ is the flame normal vector and S_d is the local flame displacement speed [30]. For taking into account the density variation in the flame zone, S_d is weighted with the density change inside the flame front $S_D = \frac{\rho}{\rho_u} S_d$, where the subscript u indicates the unburnt side of the flame. The flame displacement speed S_D can be affected by heat loss, flow non-uniformities (i.e. strain), flame curvature and the changes in local elemental composition [20]. These changes can significantly alter the flame speed which consequently can result either in a stabilized flame or in a flashback/blow-off situation. In order to characterise these changes, de Goey and Ten Thije Boonkkamp introduced a quantitative flame stretch theory [20] which takes into account the effects of stretch, heat loss and preferential diffusion on the displacement speed at the burnt side of the flame. Using integral analysis, they showed that the displacement speed at the burnt side of the flame front of stretched flames, $S_{D,b}$ is derived as [31]:

$$S_{D,b} = S_L(\psi_b)(1 - Ka), \tag{15}$$

where $\psi_b = (Z_{1,b}, \ldots, Z_{N_{e,b}-1}, h_b)$ represents the state at the burnt side of the flame in terms of elemental atomic composition for $j = 1, \ldots, N_e - 1$ elements in the mixture, and the enthalpy. Eq. (15) describes that the displacement speed at the burnt side $S_{D,b}$ of a stretched flame can be described by the flame speed of a stretchless flame $S_L(\psi_b)$ with enthalpy and composition on the burnt side of such a stretchless flame and direct stretch effects indicated by the Ka term. This relation holds for weak as well as strong stretch rates. The Karlovitz integral Ka is a non-dimensional stretch rate and given by:

$$Ka = \frac{1}{(\sigma_b \rho_u S_L)} \int_{s_u}^{s_b} \sigma Y K \rho ds, \tag{16}$$

where K is the mass based stretch rate and is linked to the displacement speed S_d via the continuity equation as $\nabla\cdot(\rho S_d \mathbf{n}) = -\rho K$ in the flame coordinate system [30]. The Karlovitz integral Ka is an integral from the unburnt s_u to the burnt side of the flame s_b. Y is a normalized reaction progress variable given as $Y = \frac{Y_f - Y_{f,u}}{Y_{f,b} - Y_{f,u}}$ with $Y_f = Y_{\mathrm{CH_4}}$ in the present study. κ is the curvature of the flame, related to the curvature of a small flame segment σ by $\kappa = \nabla\cdot\mathbf{n} = \frac{1}{\sigma}\frac{\partial\sigma}{\partial s}$. Linearisation of Eq. (15) around the adiabatic undistorted state $\psi_b^0 = (Z_{j,b}^0, h_b^0)$ with laminar flame speed $S_L = \frac{m_b^0}{\rho_b}$, results in an expression that is valid only for weakly stretched flames:

$$\frac{S_{D,b}}{S_L} = 1 - Ka + \Delta h_b \frac{\partial}{\partial h_b^0}(\ln m_b^0) + \sum_{j=1}^{N_e} \Delta Z_{j,b} \frac{\partial}{\partial Z_{j,b}^0}(\ln m_b^0)\ .$$

The first two terms on the right hand side of Eq. () describe the direct stretch effect on the flame displacement speed. The third term describes the effect of the change in enthalpy resulting from heat loss/gain and Lewis number effects while the fourth term describes the effect of changes in Z_j caused by preferential diffusion. Thus, Eq. () gives an explicit relation combining the effects of stretch rate, heat loss and preferential diffusion on the flame displacement speed. Eq. () can be further written as:

$$\frac{S_{D,b}}{S_L} = 1 - Ka + \sum_j \Delta\psi_j \cdot c_j\ . \tag{17}$$

The so-called sensitivity coefficients $c_j = \frac{\partial \ln m_b^0}{\partial \psi_j}$, with $\psi = (Z_1, \ldots, Z_{N_e-1}, h)$, are computed by varying the inlet composition and temperature of unstretched adiabatic one-dimensional flames and solving the overdetermined system $\Delta\psi_{kj} c_j = \frac{S_k^0}{S^0(\psi^0)} - 1$, by using a least squares fit [31]. The sensitivity coefficients are presented in Table 3 for enthalpy and the three elemental mass fraction changes at $\phi = 0.68$ for methane-air flames. The sensitivity coefficient of oxygen c_O has a small value as compared to the hydrogen and carbon sensitivity coefficients. This results from the fuel lean conditions implying that changes in H and C, which make up the fuel composition, have more impact on the flame displacement speed. These sensitivity coefficients will allow the quantitative separation of contributors to flame displacement speed, as presented in the next subsections.

Table 3
Sensitivity coefficients for $\phi = 0.68$ for CH_4/air flame.

$c_h[gJ^{-1}]$	c_C	c_H	c_O
2.5	133	165	1.4

4.1. Validation of prediction of flame speed using theory with simulations

In order to evaluate the changes in enthalpy and elemental mass fractions, reference values need to be computed. These reference values are taken from the undistorted adiabatic unstretched flat flame inside the reaction zone of the flame. For evaluating the Karlovitz integral Ka, the flame structure needs to be resolved and local flamelet paths have to be constructed. Such a construction results in profiles of σ, ρK, S_d/S_L and Y along the flamelet paths. Using Eq. (17) with sensitivity coefficients from Table 3 and values of $\sum_j \Delta\psi_j$ and Karlovitz integrals from numerical solutions for flashback cases for $\hat{R} = 0.79$ and $\hat{R} = 6.3$ flame holders, a validation of the theoretical estimation along the flame length is presented in Fig. 11. First, for $\hat{R} = 0.79$, it can be observed that there is an excellent agreement between $S_{D,b}/S_L$ from numerical simulations and theory. Flame speed at all axial locations is predicted well. Second, we can observe the contributions from stretch, enthalpy and preferential diffusion effects. Stretch contribution first increases, reaches a peak, and then decreases towards the downstream locations. Negative enthalpy contribution is present for a small region near the leading edge and quickly rises to the adiabatic value. Preferential diffusion contribution decreases from the leading edge towards the downstream location. For $\hat{R} = 6.30$ flashback flame, again an excellent comparison between numerics and theory throughout the flame length can be observed. Contributions to the flame speed follow similar trends as for $\hat{R} = 0.79$ except for the enthalpy contribution, which after a highly negative contribution at the leading edge, increase to a net positive contribution at the location of maximum stretch. This happens as a result of stronger pre-heating effects for wider flame holders.

The displacement speed at the burnt side $S_{D,b}$ at the anchoring location is plotted for almost 38 stable cases for 8 flame holder sizes presented in Fig. 12. It can be seen that $S_{D,b}/S_L$ for various flame holders varies from 0.4 to 1.03. It can also be observed that there is an excellent agreement between prediction from the theoretical relation using separate contributions and from direct numerical simulation results. This indicates that the theoretical relation can be used for a deeper understanding of underlying contributions to the flame speed, especially at the limit conditions.

4.2. Contributions to the flame displacement speed for different flame holders

In this subsection, the contributions to $S_{D,b}/S_L$ from stretch, preferential diffusion and enthalpy changes are analyzed at the an-

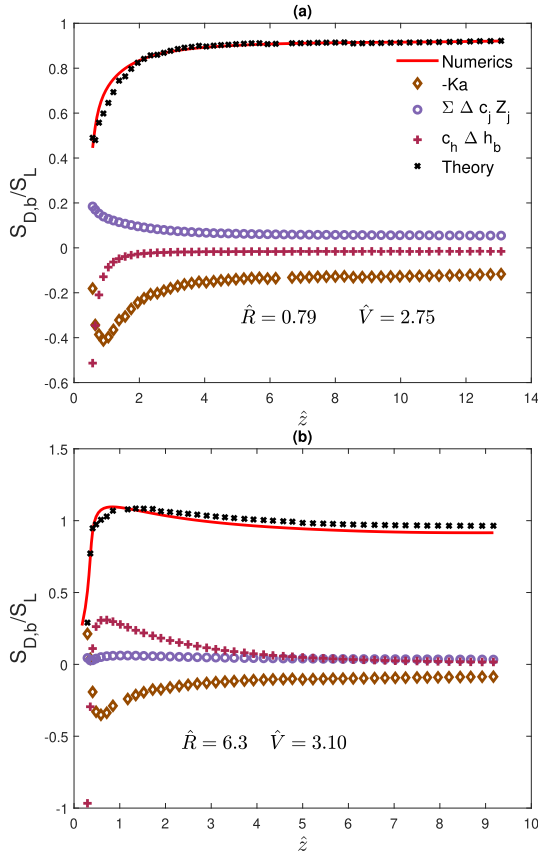

Fig. 11. Comparison between $S_{D,b}/S_L$ from numerical simulations and predicted from Eq. (17) at various axial locations for flashback limit of $\hat{R} = 0.79$ (a), bottom: $\hat{R} = 6.3$ (b) flame holders.

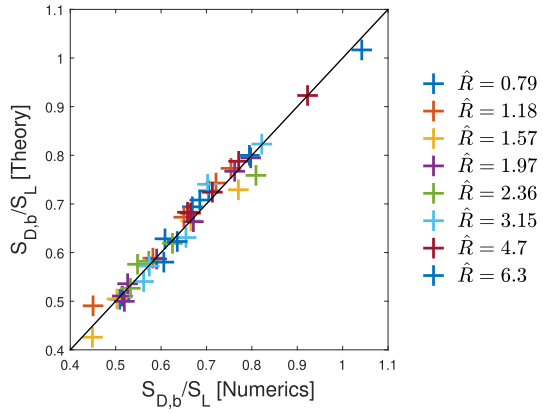

Fig. 12. Comparison between $S_{D,b}/S_L$ from numerical simulations and predicted from Eq. (17) at the location of maximum stretch (anchoring location) for all the flames presented in Table 2.

choring location. Quantification of the different terms in Eq. (17) is shown in Fig. 13 for $\hat{R} = 0.79 - 6.3$ with varying normalized rim velocity $\hat{V}$. Results are plotted from the flashback to the blow-off limit for $\hat{R} = 0.79 - 1.57$, and from flashback to the regime transition limit for $\hat{R} = 1.97 - 6.3$. Here, it can be seen that for $\hat{R} = 0.79$, with increasing $\hat{V}$, the Karlovitz integral Ka increases. This negative contribution from direct stretch to $S_{D,b}$ is countered by stretch induced preferential diffusion effects which increase with $\hat{V}$. The net effect of these contributions is dominated by the direct stretch effect ($-Ka$) which reduces $S_{D,b}$. The heat loss to the flame holder, which decreases with an increase in flow velocity for flames stabilized without a RZ [1], also results in less pre-heating reaching the flame anchoring location as observed in Fig. 8. This causes a diminishing support to the anchoring location just downstream of the heat loss affected leading edge and results in a flame that is still subjected to a net heat loss as evident from the negative enthalpy contribution at the anchoring location. It is to be noted here changes in enthalpy contribution from Lewis number effects are small compared to that from heat transfer. With further increase in the inlet velocity, the flame blows off. Similar trends can be observed for $\hat{R} = 1.18 - 1.57$ where the velocity at which blow-off happens increases with an increase in flame holder size. For these cases, the flame near blow-off is subjected to an increasing stretch contribution while the enthalpy contribution tends to flatten when approaching the blow-off limit.

For flames stabilized on flame holders with $\hat{R} = 1.97 - 6.3$, the different contributions to $S_{D,b}$ are also shown in Fig. 13. With increasing mixture velocity from the flashback limit, blow-off does not happen here but the flame enters the RZ stabilization regime. For $\hat{R} = 1.97$, trends similar to that for flames stabilized on $\hat{R} < 1.6$ flame holders are observed for stretch, preferential diffusion and enthalpy. The stretch contribution $-Ka$ increases with an increase in $\hat{V}$ but the increase is less than that was observed for $\hat{R} = 1.57$. The enthalpy contribution then decreases towards the emergence of a RZ in a similar manner as for the $\hat{R} < 1.6$ stabilized flames. For $\hat{R} = 2.36 - 6.3$, a higher pre-heating effect is observed at the flashback limit, corresponding to a higher heat loss to the top face of the flame holder. The impact of these changes on flashback, blow-off and transition to RZ stabilization regime limits is discussed in the next subsections as a function of normalized flame holder radius $\hat{R}$.

4.3. Flashback mechanism

In this subsection, the changing trends of stretch, enthalpy and preferential diffusion contributions at the flashback limit for different flame holders are summarized. These contributions at the flashback limit are plotted together in Fig. 14 for the eight radii analyzed in this study. These results can be analyzed together with those from Fig. 13 for a more detailed understanding of flame flashback for the presented cases. Linear fits for each data line is also represented as some scatter exists possible due to uncertainty in the limit calculation.

It can be seen in Fig. 14 that the stretch contribution ($-Ka$) for all flame holders is almost constant at the flashback limit. The contribution of stretch induced preferential diffusion is highest for $\hat{R} = 0.79$ and decreases with an increase in $\hat{R}$ but the slope of this change is small. The most drastically changing contribution, however, is from the enthalpy change, which changes sign as $\hat{R}$ is increased and correlates in a good manner with change in $S_{D,b}$ shown by the black curve. This happens as more heat is lost to the flame holder for higher $\hat{R}$, resulting in stronger pre-heating of the anchoring region. This effect is less profound for lower $\hat{R}$. It can be argued from this discussion that for flame holders of varying sizes, displacement speed at the flame flashback limit is a strong function of enthalpy change contribution i.e. $(S_{D,b})_{FB} \propto c_h \Delta h_b$.

In summary, extrapolating from Fig. 13, and using Fig. 14, with further decrease in mixture velocity, flashback happens:

- for smaller flame holders, because the local $S_{D,b}$ becomes higher than the flow velocity primarily due to lack of stretch. In other words, if the stretch rate could be further increased, flame flashback would happen at a lower mixture velocity. Due

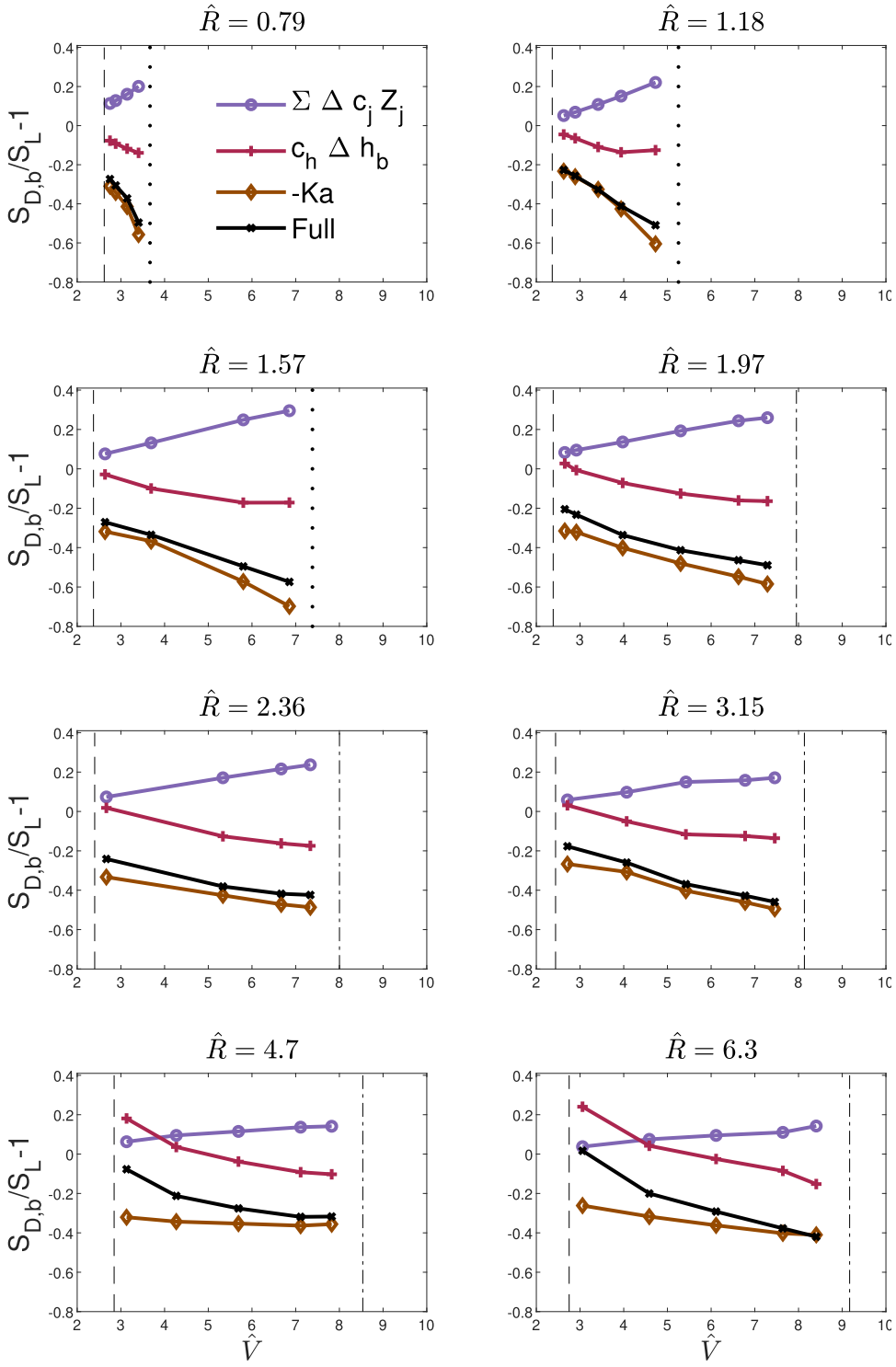

Fig. 13. Different contributions to displacement speed $S_{D,b}/S_L$ as per Eq. (17) at the location of maximum stretch near the flame base region for flames stabilized without RZ.– – –, . . . and –. lines represent computed conditions at which flashback, blow-off and regime transition occurs.

to relatively low heat loss because of the small flame holder top surface area, $S_{D,b}$ is not enhanced in a significant manner by the pre-heating effect.

- for larger flame holders, the local $S_{D,b}$ becomes higher than the flow velocity due to an increase in enthalpy (change) contribution (by pre-heating) to the flame speed as the flame and burnt gases lose heat to the burner with larger surface area coupled with low stretch rates.

4.4. Blow-off mechanism

In this subsection, blow-off (in the absence of a RZ) for $\hat{R} < 1.6$ flame holders is analysed. Contributions to $S_{D,b}$ at the anchoring location at blow-off limit are plotted in Fig. 14 as a function of $\hat{R}$. Note that blow-off velocities increase with increase in flame holder radius. We can observe that the contribution from enthalpy change almost remains constant with changing flame holder radius. This

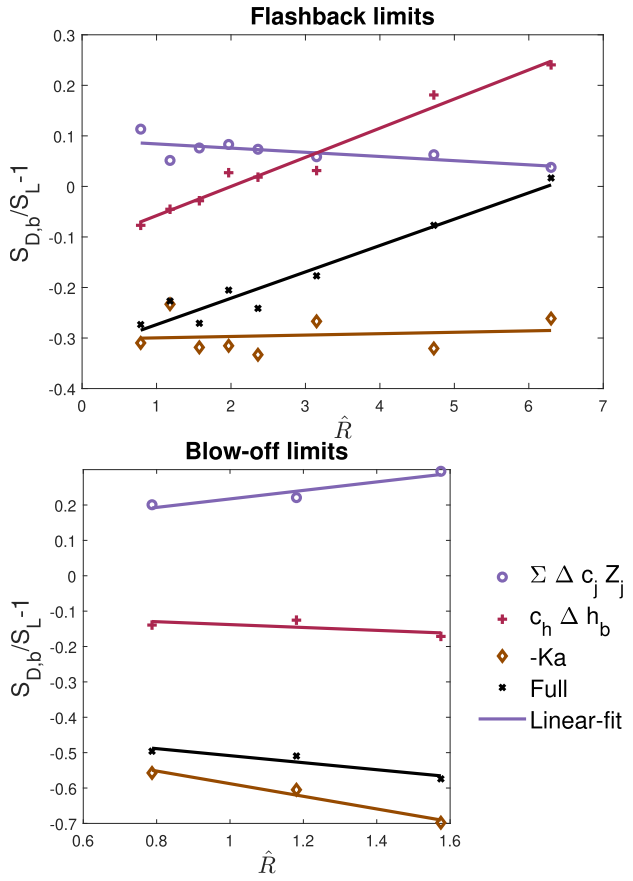

Fig. 14. Different contributions to displacement speed $S_{D,b}/S_L$ as per Eq. (17) at the flame anchoring location for flashback (top) and blow-off (bottom) limit flames as a function of flame holder radius.

happens due to the observed flattening of the enthalpy contribution curve in Fig. 13 at the blow-off limit. The stretch contribution at the flame anchoring location increases due to an increased flow strain rate [1] along with an increase in preferential diffusion contribution. The result of these two contributions determines the trend of flame speed at blow-off for various flame holders.

Extrapolating from Fig. 13 and using Fig. 14, with further increase in mixture velocity, blow-off occurs because:

- The stretch rate near the flame base increases due to an increased flow strain rate, and the heat loss to the burner decreases.
- This results in less pre-heating support to the region of highest stretch rate such that the flame speed decreases with increasing $\hat{V}$.
- Blow-off occurs as a result of any further increase in stretch rate and a decrease in heat loss causing the pre-heating flame support to become insufficient.
- With increasing flame holder radius, the flame experiences a higher stretch contribution near the flame anchoring location, while the blow-off limit is extended. This extension is caused by the flattening of the enthalpy contribution at a higher flow velocity due to the higher flame holder top surface area. In other words, pre-heating support to the flame anchoring location, which increases with an increase in flame holder radius, pushes the blow-off limit to a higher flow velocity.

It must be stressed here that blow off for the presented cases does not happen in an anomalous manner such as observed in Ref. [12,17,32,33] (for flame neck location), but due to a decrease in flame speed caused by the stretch rate. It should be clear from the discussion presented here that blow-off behaviour without a RZ is dominated by an interplay between heat loss, pre-heating and stretch (including preferential diffusion) near the flame base region varying with inlet velocity and flame holder radius. Their combined effect makes the flame blow off with an increase in the mixture velocity but stretch rate appears to strike the final blow in pushing the flame away from the flame holder.

4.5. Transition to RZ stabilization regime

In this subsection, (apart from flashback and blow-off) a third scenario is discussed, i.e., the emergence of a RZ with an increase in mixture velocity and transition to RZ stabilized regime. In the previous subsection, we discussed how an increase in the flame holder radius can delay flame blow-off to a higher velocity by increased pre-heat support (resulting from an increased heat loss with an increase in flame holder top surface area). For cases when the flame holder radius and flow velocity are large enough, blow-off is prevented by the transition to the RZ stabilized regime [1]. For $\hat{R} = 1.96 - 6.3$ flames, at the regime transition limit, contributions to flame displacement speed at the anchoring location are plotted in Fig. 15 along with linear fits as a function of flame holder radius. Here, *Ka* decreases with an increase in the flame holder radius, contrary to the blow-off cases. Consequently, the preferential diffusion contribution also decreases with an increase

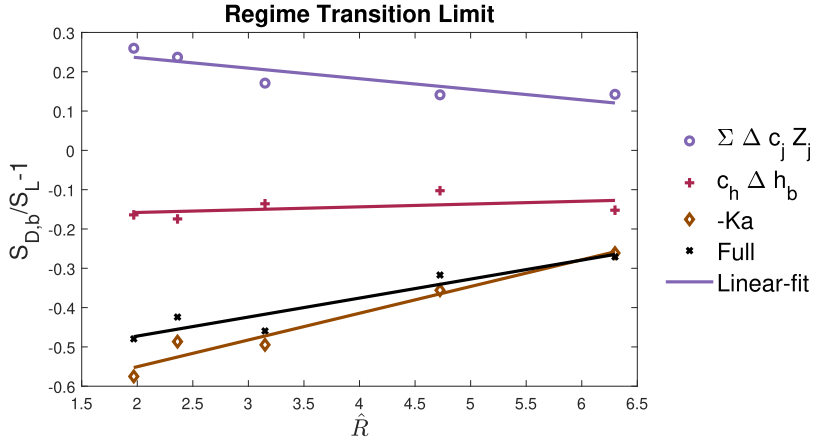

Fig. 15. Different contributions to displacement speed $S_{D,b}/S_L$ as per Eq. (17) at the location of maximum stretch near the flame anchoring location for flames transitioning to RZ stabilized regime.

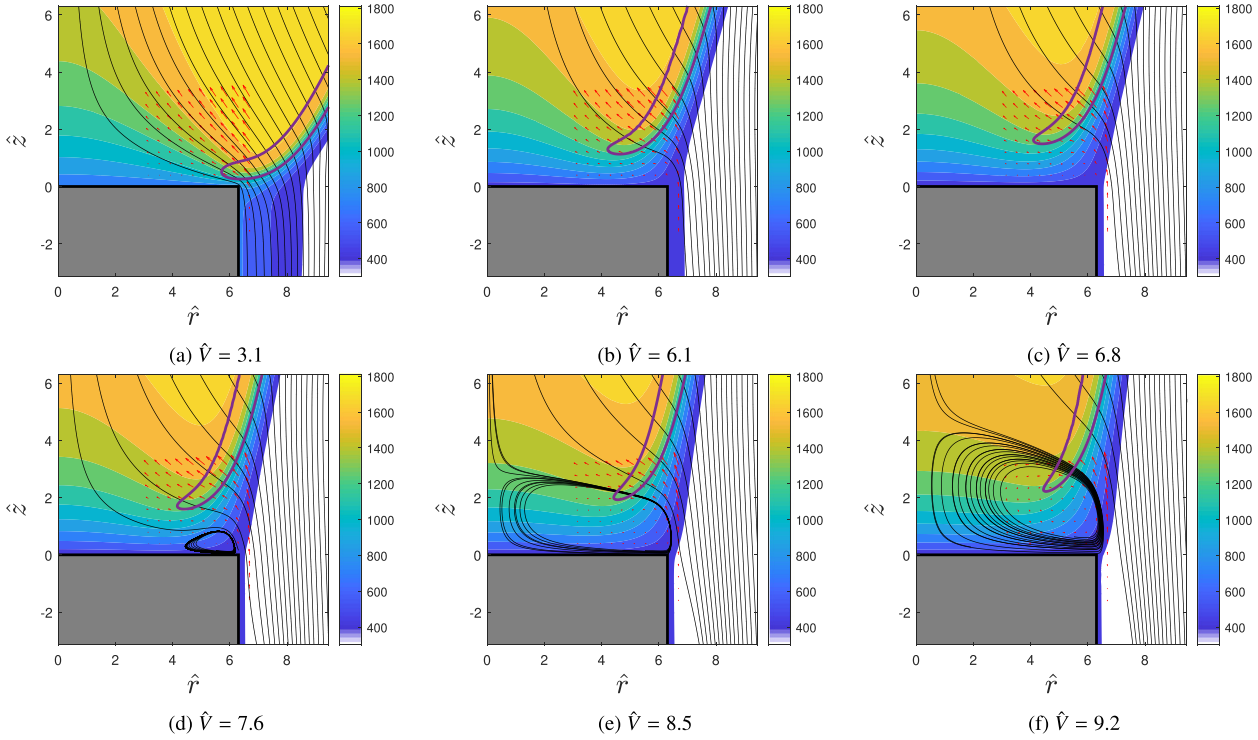

Fig. 16. Streamlines and iso-contour of 10 percent of maximum heat release rate (in purple) along with flow vectors (red) near flame holder corner for $\hat{V} = 3.1 - 9.2$ for $\hat{R} = 6.3$ against background temperature contours. (For interpretation of the references to color in this figure legend, the reader is referred to the web version of this article.)

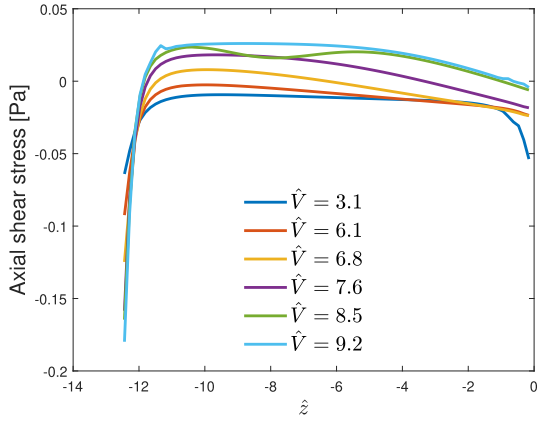

Fig. 17. Axial shear stress on the side wall for cases presented in Fig. 16 for $\hat{R} = 6.3$ flame holder.

in $\hat{R}$. The enthalpy contribution again appears to be constant for all limit cases. Due to the decreasing heat loss to the flame holder with an increase in $\hat{V}$, less pre-heating support reaches the flame base, similar to the blow-off scenarios for the $\hat{R} < 1.6$ flames. This increases the flame stand-off distance from the top face of the flame holder. Instead of blowing-off, a RZ appears due to an additional flame-flow interaction, causing the flames to remain stabilized. This flame-flow interaction that results in the emergence of a RZ, is discussed next.

The flow structure near the flame leading edge for $\hat{R} = 6.3$, is shown in Fig. 16(a–f) for increasing velocities from the flashback limit to the point where a RZ emerges. It can be observed from the flow vectors for the low velocity case ($\hat{V} = 3.1$) in Fig. 16(a) that due to the close proximity of the flame to the flame holder corner, the flow does not separate and results in suppression of the RZ due to thermal expansion of the gas in the flame represented by temperature contours.

With increasing mixture velocity in Fig. 16(b-c), the flame leading edge moves away from the flame holder and the temperature gradient between them causes a weaker thermal expansion than for $\hat{V} = 3.1$. This decreases the diversion of the flow in radial direction towards the axis of symmetry, but this diversion is still enough for the suppression of a RZ even when the cold flow Reynolds number increases. In Fig. 16(d), a RZ (bubble) can be observed to emerge at the flame holder corner because the inertial forces which start to dominate the flow divergence in the thermal boundary layer. At this velocity ($\hat{V} = 7.6$), the flame leading edge is outside the RZ and thus it is stabilized without any significant interference to the stretch and heat loss stabilization mechanism described in the previous sections. For a higher inlet velocity, the RZ becomes larger as the flame stand-off distance increases further. For $\hat{V} = 8.5$, the flame leading edge starts to interact with the RZ. A further increase in $\hat{V}$ allows the flame to enter the RZ-stabilized flame mechanism as observed in Fig. 16(f) reversing the heat loss trend with an increase in $\hat{V}$. Axial shear stress on the side wall is shown in Fig. 17 for the same $\hat{V}$ as in Fig. 16. It can be observed that for $\hat{V} = 3.1$ to $\hat{V} = 6.8$, axial shear stress on the side wall is negative at almost all locations indicating that no flow-separation has occurred. For $\hat{V} > 6.8$, positive axial shear stress on the upstream side of the wall can be observed indicating that flow separation is present at the side wall. This flow separation coupled with thermal expansion near the corner of flame holder determines if the flame stabilizes in the RZ stabilized regime or not.

The emergence of a RZ can be summarized (based on Figs. 13, 15 and 16) as follows: As the velocity $\hat{V}$ is increased from the flashback limit,

- the heat loss to the flame holder decreases, causing the flame stand-off distance to increase.

- The thermal boundary layer between the flame holder and flame suppresses flow separation at the flame holder corner due to flow acceleration.
- With further increasing $\hat{V}$, inertial forces dominate and a RZ emerges causing the flame to switch stabilization mechanism.
- The regime transition velocity is found to be a function of V_{rim}/S_L for different flame holder sizes rather than the Reynolds number, as would be the case with non-reacting flow situations.

5. Summary and conclusions

In this study, a systematic analysis of the stabilization of premixed flames in the absence of a RZ is presented. An anchoring location where the stretch rate is maximum along the flame front is identified as a more representative anchoring location than the flame leading edge. Near the flashback limit, flames stabilized on flame holders of different radii were found to be stable without the presence of a RZ, even when the radius of the flame holder is 6 times greater than the flame thickness. For high velocities, flames are found to blow-off for $\hat{R} < 1.6$, while for $\hat{R} > 1.6$ they transition to RZ stabilized regime with increasing mixture velocity.

The mechanisms leading to flame flashback, blow-off and transition to RZ regime are analyzed quantitatively by using flame stretch theory. Contributions to the flame displacement speed from stretch, stretch induced preferential diffusion and enthalpy changes at the anchoring location are used for interpretation of different limit mechanisms. Flames stabilized on flame holders of smaller radius show flashback as a result of a decrease in stretch rate, while for larger radii, flashback happens as a result of stronger pre-heating effects, when the flow velocity is decreased. Flame speed at flashback as a function of flame holder radius is found to correlate well with enthalpy changes.

Blow-off happens in a more complicated manner. With increasing inlet velocity, flame stand-off distance increases resulting in a decrease in heat loss to the flame holder. With decreasing heat loss, pre-heating by conduction through the flame holder decreases and the flame is not supported at the locations of high stretch. A further increase in the inlet velocity results in an increase in the stretch rate, thus reducing the flame speed and resulting in flame blow-off.

For flame holders with larger radius, due to higher heat loss and thus higher pre-heating support to the anchoring location, the flame does not blow-off. This, coupled with flame stand-off distance increasing along with inertial forces, allows for the emergence of recirculation zone behind the flame holder. Beyond this velocity, the flame transitions to recirculation zone stabilized regime.

The major outcome of this study is the presentation of an in-depth understanding of the flame stabilization mechanism of CH_4/air flame when a recirculation zone is not present. Results from this study are expected to contribute towards the development of a generalized flame stabilization theory that can take into account the specific physical effects associated with flame holder geometries of various sizes.

Declaration of Competing Interest

The authors declare that they have no known competing financial interests or personal relationships that could have appeared to influence the work reported in this paper.

Acknowledgments

The authors would like to express their gratitude to the Netherlands Organisation for Scientific Research (NWO) for their financial support under Project no. 13549.

References

[1] F.H. Vance, Y. Shoshin, L.P.H. de Goey, J.A. van Oijen, Flame stabilization regimes for premixed flames anchored behind cylindrical flame holders, Proc. Combust. Inst. 38 (2021) 1983–1992.
[2] E.E. Zukoski, F. Marble, Experiments concerning the mechanism of flame blow-off from bluff bodies, Proc. Combust. Inst. (1983).
[3] E. Zukoski, Flame Stabilization on Bluff Bodies at Low and Intermediate Reynolds Number, California Institute of Technology, 1954 PhD Thesis.
[4] K.S. Kedia, A.F. Ghoniem, The anchoring mechanism of a bluff-body stabilized laminar premixed flame, Combust. Flame 161 (2014) 2327–2339.
[5] K.S. Kedia, A.F. Ghoniem, The blow-off mechanism of a bluff-body stabilized laminar premixed flame, Combust. Flame 162 (2015) 1304–1315.
[6] F. Williams, Combustion Theory, Westview Press, 1994.
[7] S. Chaudhuri, S. Kostka, M.W. Renfro, B.M. Cetegen, Blowoff dynamics of bluff body stabilized turbulent premixed flames, Combust. Flame 157 (2010) 790–802.
[8] B.J. Lee, C.S. Yoo, H.G. Im, Dynamics of bluff-body-stabilized premixed hydrogen/air flames in a narrow channel, Combust. Flame 162 (2015) 2602–2609.
[9] F.A. Williams, Flame stabilization of premixed turbulent premixed gases, Appl. Mech. Surv. (1966) 1157–1170.
[10] S.J. Shanbhogue, S. Husain, T. Lieuwen, Lean blowoff of bluff body stabilized flames: scaling and dynamics, Prog. Energy Combust. Sci. (2009) 98–120.
[11] M. Miguel-Brebion, D. Mejia, P. Xavier, F. Duchaine, B. Bedat, L. Selle, T. Poinsot, Joint experimental and numerical study of the influence of flame holder temperature on the stabilization of a laminar methane flame on a cylinder, Combust. Flame 172 (2016) 153–161.
[12] F.H. Vance, Y. Shoshin, J.A. van Oijen, L.P.H. Goey, Effect of lewis number on premixed laminar lean-limit flames stabilized on a bluff body, Proc. Combust. Inst. 37 (2019).
[13] V.N. Kurdyumov, Y. Shoshyn, L. de Goey, Structure and stability of premixed flame stabilized behind the trailing edge of a cylindrical rod at low lewis numbers, Proc. Combust. Inst. 35 (2015) 981–988.
[14] B. Lewis, G. von Elbe, Stability and structure of burner flames, J. Chem. Phys. 11 75 (1943).
[15] C.J. Sung, C.K. Law, A. Umemura, On adiabatic stabilization of inverted flames, 24th Symposium (International) on Combustion (1992), pp. 205–212.
[16] T. Kawamura, K. Asato, T. Mazaki, T. Hamaguchi, H. Kayahara, Explanation of the blowoff of inverted flames by the area-Increase concept, Combust. Flame 35 (1979) 109–116.
[17] Y. Shoshin, R.J.M. Bastiaans, L.P.H. de Goey, Anomalous blow-off behavior of laminar inverted flames of ultra-lean hydrogen-methane-air mixtures, Combust. Flame 160 (2013) 565–576.
[18] K. Kedia, A. Ghoniem, Mechanisms of stabilization and blowoff of a premixed flame downstream of a heat-conducting perforated plate, Combust. Flame 159 (2012) 1055–1069.
[19] T. Kawamura, K. Asato, T. Mazaki, Reexamination of the blowoff mechanism of premixed flames-Inverted flames, Combust. Flame 45 (1982) 225–233.
[20] L.P.H. de Goey, J.H.M. ten thije Boonkkamp, A flamelet description of premixed laminar flames and the relation with flame stretch, Combust. Flame 119 (1999) 253–271.
[21] F.H. Vance, Y. Shoshin, J.A. van Oijen, L.P.H. Goey, The effect of thermal diffusion on stabilization of premixed flames, Combust. Flame 216 (2020) 45–57.
[22] Ansys fluent, release 17.2
[23] A. Kazakov, M. Frenklach, Reduced reaction sets based on GRI-Mech 1.2http://combustion.berkeley.edu/drm/.
[24] M.D. Smooke, V. Giovangigli, Formulation of the Premixed and Nonpremixed Test Problems, Springer Verlag, Berlin, 1991, p. 128.
[25] J.A. van Oijen, Flamelet-generated Manifolds : Development and Application to Premixed Laminar Flames, 2002 PhD thesis.
[26] CHEM1D. A one dimensional laminar flame code. eindhoven university of technology (????).
[27] T. Poinsot, D. Veynante, Theoretical and Numerical Combustion, second ed. (????).
[28] C.K. Law, Combustion physics, Cambridge University Press (2006).
[29] T.C. Lieuwen, Unsteady Combustor Physics, Cambridge University Press, 2012.
[30] L.P.H. de Goey, R.M.M. Mallens, J.H.M. ten thije Boonkkamp, An evaluation of different contributions to flame stretch for stationary premixed flames, Combust. Flame 110 (1997) 54–66.
[31] J.A. van Oijen, A. Donini, R.J.M. Bastiaans, J.H.M. ten thije Boonkkamp, L.P.H. de Goey, State-of-the-art in premixed combustion modeling using flamelet generated manifolds, Prog. Energy Combust. Sci. 57 (2016) 30–74.
[32] J. Wan, H. Zhao, Blow-off mechanism of a holder-stabilized laminar premixed flame in a preheated mesoscale combustor, Combust. Flame 220 (2020) 358–367.
[33] C. Jimenez, D. Michaels, A.F. Ghoniem, Stabilization of ultra-lean hydrogen enriched inverted flames behind a bluff-body and the phenomenon of anomalous blow-off, Combust. Flame 191 (2018) 86–98.